Lattice Boltzmann method for compressible Euler equations based on exact kinetic system

Hanada, Takaya

Kataoka, Takeshi

(Citation)
International Journal for Numerical Methods in Fluids,93(8):2554-2569

(Issue Date)
2021-08

(Resource Type)
journal article

(Version)
Accepted Manuscript

(URL)
https://hdl.handle.net/20.500.14094/90008415

LATTICE BOLTZMANN METHOD FOR COMPRESSIBLE EULER EQUATIONS BASED ON EXACT KINETIC SYSTEM

Takaya Hanada and Takeshi Kataoka

Corresponding author: Takeshi Kataoka
Graduate School of Engineering, Kobe University
Rokkodai, Nada, Kobe 657-8501, Japan
E-mail: kataoka@mech.kobe-u.ac.jp

SUMMARY

We have developed a new type of simple lattice Boltzmann (LB) model for the compressible Euler equations based on the collisionless kinetic-equation approach proposed by Sone[1]. The model uses the collisionless kinetic equation in the streaming process, and modifies the distribution function to its Chapman-Enskog type at each time step. Compared with the current LB models which solve the kinetic equation of the BGK type, the proposed model is superior in the following two points: (i) Inviscid flows can be computed stably while there is no such model in the current LBM; (ii) The velocity distribution function does not need to be memorized in computation. We calculate various inviscid compressible flows described by the compressible Euler equations using our new 1D, 2D and 3D models. Numerical results show the capability of our scheme to simulate high-speed supersonic flows with shock waves.

Keywords: Compressible flow, Lattice Boltzmann, Supersonic, Euler flow, Computational method, Shock wave

1. INTRODUCTION

The lattice Boltzmann method (LBM)[2-23]is one of well-known numerical methods to obtain solutions of the fluid-dynamic-type equations. The LBM solves the kinetic equation with a finite number of molecular velocities such that the macroscopic variables obtained from the solution satisfy the desired fluid-dynamic-type equations. The merits of the LBM are the simple basic equation, the linear derivative terms, high resolution for capturing discontinuities like shock waves[3,6-17] and small oscillations like sound waves[18-21]. Owing to these merits, the LBM is already a matured numerical tool for simulating various flows. However, the LBM still has the following defects as a numerical tool:

(i) There exists a relaxation time in the denominator of collision term of BGK equation (as noted in Sone[1]), so that it is impossible to compute inviscid flows for which the relaxation time is zero.

(ii) Additional computer memory is necessary in the computation of the current LBM because not only macroscopic variables but also the velocity distribution function must be memorized.

Regarding (i), some researchers resorted to multiple-relaxation-time (MRT) models and succeeded in overcoming this difficulty[22,23]. However, the MRT model is a little complicated due to the complexity of transformation matrix. Concerning (ii), Inamuro[24] devised such a model for incompressible flows, but there is no model for compressible flows. So it is necessary to develop a LB model that can simulate supersonic inviscid flows for which the relaxation time is zero, and no additional memory for the velocity distribution function is required.

Sone[1] proposed a simple idea to construct a kinetic system of a 'collisionless' kinetic equation in which there is no relaxation time included. On the basis of this system, he discussed a simpler scheme than the current LB models. The key is to modify the velocity distribution function at each time step to Chapman-Enskog type. His theory uses continuous molecular velocities so that there still needs a work to be done as a numerical solver to introduce discrete molecular velocities. If we are successful in developing this new model, we can overcome either of the above-mentioned issues (i) and (ii) of the current LBM.

There is another line of studies on the kinetic equation approach, which is called gas-kinetic scheme, by evaluating the fluxes of fluid-dynamic-type equations on the basis of kinetic theory. Pullin[25] first constructed such a scheme for the Euler equations[26] and Chou & Baganoff[27] devised the corresponding NS model. Basically, these gas-kinetic schemes utilize the continuous velocity distribution function which is Maxwellian at the leading order[28-34]. Since we need to use prohibitively many meshes to solve the kinetic equation of continuous molecular velocities, they avoid such computation and evaluate the moments of velocity distribution function (the fluxes) analytically. In this analytical process, some involved techniques including local redistribution process are necessary. To remedy this, some simplifying methods have been also proposed: Yang et al. [35,36] introduced modified equilibrium distribution functions of a circular or spherical type instead of the conventional Maxwellian. Their method reduced the complexities of the kinetic scheme arising at the cell interface.

Our model presented in this study is fundamentally different from the above gas-kinetic scheme. That is, the velocity distribution function is 'discrete' in the molecular velocity space. We use a function that is expressed by the collection of 'delta functions' in molecular velocity space (see (25) below). This makes it possible to compute the

kinetic equation directly because the number of meshes in the molecular velocity space is reduced to allowable finite numbers.

To sum up, the merits of our model are:

(I) There is no collision term so that we can compute inviscid flows for which the relaxation time is zero.

(II) The macroscopic variables can be calculated without the velocity distribution function so that there is no need to store the velocity distribution function, while the current LB models need to store the velocity distribution function.

(III) The scheme is 'simple'. It is not necessary to reconstruct a local solution at each time step.

Here, (I) and (II) come from a comparison against the current LB models, while (III) is against the gas kinetic schemes. In fact, we already succeeded in constructing the model with these three merits for computing subsonic (viscous) flows[21]. This paper is therefore concerned with devising the corresponding scheme for supersonic (inviscid) flows with shock waves. This is the first study to develop such a LB model of a collisionless equation that can compute supersonic flows.

To summarize, we propose a new type of lattice Boltzmann (LB) model for the compressible Euler equations that can compute supersonic flows and are novel in (I)-(III). To devise such model, we will make the system by Sone[1] effective as a numerical solver by introducing discrete molecular velocities and the corresponding Chapman-Enskog-type velocity distribution function explicitly. The number and position of molecular velocities are dependent on the fluid-dynamic-type equations we want to solve, which are the compressible Euler equations here. They are looked for under the constraint that some moments of the velocity distribution function satisfy the prescribed relations (see (24) below).

The present paper is arranged in the following order. In Section 2 the kinetic system proposed by Sone[1] is briefly explained, and in Section 3 new LB model for the compressible Euler equations is presented. The role of error term is discussed in Section 4. Numerical examples are shown in Section 5. Concluding remarks follow in Section 6.

2. KINETIC SYSTEM DEVELOPED BY SONE

The key point of this paper is an introduction of a discrete velocity distribution function with discrete molecular velocities that enables us to compute the kinetic equation directly within an acceptable computational cost. Before going into such new discrete model, we here summarize the kinetic-equation approach devised by Sone[1]. Section 2.1 explains an exact system and Section 2.2 treats a simpler system that uses the collisionless equation.

2.1 Exact kinetic system

Let x_α, c_α, η, and t ($\alpha = 1, \cdots, D$; D is the number of dimensions) be independent variables, and $f(x_\alpha, c_\alpha, \eta, t)$ be the velocity distribution function. The macroscopic variables ρ_r ($r = 0, \cdots, D+1$) are defined as

$$\rho_r = \int_{-\infty}^{\infty} \cdots \int_{-\infty}^{\infty} f \phi_r \, d\boldsymbol{c} d\eta, \tag{1}$$

where $\phi_r(c_\alpha, \eta)$ ($r = 0, \cdots, D+1$) are functions of c_α (or $\boldsymbol{c}$) and η chosen appropriately. The flux H_α^r of the

macroscopic variables is defined as

$$H_\alpha^r = \int_{-\infty}^{\infty} \cdots \int_{-\infty}^{\infty} f \phi_r c_\alpha \, d\boldsymbol{c} d\eta. \tag{2}$$

Take a velocity distribution function f^c of the Chapman-Enskog type:

$$f = f^c(\rho_r, c_\alpha, \eta)\,, \tag{3}$$

where the variables x_α and t enter only through the macroscopic variables ρ_r. Here the dependence on the derivative $\nabla\rho_r$ is omitted because we are interested in constructing the Euler system (it is straightforward to incorporate the dependence on $\nabla\rho_r$ when one constructs the NS system[21]). The moments of f^c are

$$\rho_r = \int_{-\infty}^{\infty} \cdots \int_{-\infty}^{\infty} f^c \phi_r d\boldsymbol{c} d\eta, \quad H_\alpha^{rc}(\rho_r) = \int_{-\infty}^{\infty} \cdots \int_{-\infty}^{\infty} f^c \phi_r c_\alpha d\boldsymbol{c} d\eta. \tag{4}$$

Using this function f^c, Sone[1] introduced the following initial-value problem of the kinetic equation:

$$\frac{\partial f}{\partial t} + c_\beta \frac{\partial f}{\partial x_\beta} = Q, \tag{5a}$$

where

$$Q \equiv \frac{\partial f^c}{\partial \rho_r}\left(c_\beta \frac{\partial \rho_r}{\partial x_\beta} - \frac{\partial H_\beta^{rc}}{\partial x_\beta} \right), \tag{5b}$$

and the initial condition:

$$f = f^c\left(\rho_r^{(0)}, c_\alpha, \eta\right) \text{ at } t = 0\,. \tag{6}$$

Hereafter the summation convention is applied to the subscripts α, β, r. It is easy to check that Q defined by (5b) satisfies (see (4))

$$\int_{-\infty}^{\infty} \cdots \int_{-\infty}^{\infty} Q \phi_r \, dc_1 \cdots dc_D d\eta = 0\,. \tag{7}$$

Sone proved that a solution of the above initial-value problem (5) and (6) is $f = f^c$ whose macroscopic variables ρ_r are the solution of

$$\frac{\partial \rho_r}{\partial t} + \frac{\partial H_\beta^{rc}}{\partial x_\beta} = 0, \tag{8}$$

with the initial conditions:

$$\rho_r = \rho_r^{(0)} \text{ at } t = 0\,. \tag{9}$$

Thus, by choosing an appropriate Chapman-Enskog-type function f^c such that (8) agree with the desired fluid-dynamic-type equations (compressible Euler equations here), we get a desired solution of macroscopic variables.

2.2 Simple kinetic system

Let us consider to solve, instead of (5), the following simple collisionless kinetic equation

$$\frac{\partial f}{\partial t} + c_\beta \frac{\partial f}{\partial x_\beta} = 0, \tag{10}$$

in a continuous sequence of time intervals $(0, \Delta t]$, $(\Delta t, 2\Delta t]$, $\cdots$ under the initial condition for each interval $(m\Delta t, (m+1)\Delta t]$ given by

$$f = f^c\left(\rho_r^{(m)}, c_\alpha, \eta\right) \text{ at } t = m\Delta t\,, \tag{11}$$

where $\rho_r^{(0)}$ are the initial values at $t = 0$, and $\rho_r^{(m)}$ $(m \neq 0)$ are ρ_r calculated from the solution f at $t = m\Delta t$ of (10) in the preceding interval $((m-1)\Delta t, m\Delta t]$.

If the simple system (10)-(11) is compared with the exact system (5)-(6), we find that the difference between the two kinetic equations (10) and (5) lies in the collision term Q on the right-hand side of (5). In order to estimate the effect of this collision term, it is convenient to express solution of the exact system (5)-(6) in the integrated form[31] along its characteristic line of the time interval $(0, \Delta t]$ as

$$f(x_\alpha, \Delta t) = f\left(x_\alpha - c_\alpha \Delta t, 0\right) + \int_0^{\Delta t} Q\left(x_\alpha - c_\alpha(\Delta t - \tau), \tau\right) \mathrm{d}\tau\,, \tag{12a}$$

where Q is expressed, after Taylor expansion around $(x_\alpha, \Delta t)$, as

$$Q\left(x_\alpha - c_\alpha(\Delta t - \tau), \tau\right) = Q\left(x_\alpha, \Delta t\right) - (\Delta t - \tau)\left[\frac{\partial Q}{\partial \tau}\left(x_\alpha, \Delta t\right) + c_\beta \frac{\partial Q}{\partial x_\beta}\left(x_\alpha, \Delta t\right)\right] + O(\Delta t^2). \tag{12b}$$

If we use the finite-difference scheme in τ: $\partial Q / \partial \tau = \left[Q(x_\alpha, \Delta t) - Q(x_\alpha, 0)\right] / \Delta t + O(\Delta t^2)$ in (12b) and substitute the result into (12a), we find

$$f(x_\alpha, \Delta t) = f\left(x_\alpha - c_\alpha \Delta t, 0\right) + \Delta t \frac{Q\left(x_\alpha, 0\right) + Q\left(x_\alpha, \Delta t\right)}{2} - \frac{\Delta t^2}{2} c_\beta \frac{\partial Q}{\partial x_\beta}\left(x_\alpha, \Delta t\right) + O(\Delta t^3)\,. \tag{13}$$

Compared with a solution of the collisionless system $f(x_\alpha, \Delta t) = f\left(x_\alpha - c_\alpha \Delta t, 0\right)$, we readily find that the error of the velocity distribution function f using the collisionless system is $O(\Delta t)$ by one time step. Our interest here is the error of the macroscopic variables ρ_r $(r = 0, \cdots, D+1)$. To this end, one should integrate (13) in c_α and η after multiplying it by ϕ_r to get

$$\rho_r(x_\alpha, \Delta t) = \rho_r\left(x_\alpha - c_\alpha \Delta t, 0\right) - \frac{\Delta t^2}{2} \frac{\partial}{\partial x_\beta} \int_{-\infty}^{\infty} \cdots \int_{-\infty}^{\infty} Q \phi_r c_\beta dc_1 \cdots dc_D d\eta + O(\Delta t^3)\,, \tag{14}$$

where (7) is used. Thus, the error of the macroscopic variables is $O(\Delta t^2)$ by one time step and $O(\Delta t)$ at a finite time which can be made sufficiently small according to our convenience. There is no intrinsic error proportional to the flow parameters which exists in the current LBM.

3. NEW LB MODEL

We now present a new LB model for the compressible Euler equations. Let us first write down an initial-value

problem of the compressible Euler equations that we want to solve:

$$\frac{\partial \rho}{\partial t}+\frac{\partial \rho u_\alpha}{\partial x_\alpha}=0\,, \tag{15a}$$

$$\frac{\partial \rho u_\alpha}{\partial t}+\frac{\partial \rho u_\alpha u_\beta}{\partial x_\beta}=-\frac{\partial p}{\partial x_\alpha}\,, \tag{15b}$$

$$\frac{\partial \rho\left(bRT+u_\beta^2\right)}{\partial t}+\frac{\partial \Pi_\alpha}{\partial x_\alpha}=0\,, \tag{15c}$$

where

$$p=\rho RT,\qquad \Pi_\alpha=\rho\left(bRT+u_\beta^2\right)u_\alpha+2pu_\alpha\,, \tag{15d}$$

with the initial conditions

$$\rho=\rho^{(0)},\ u_\alpha=u_\alpha^{(0)},\ T=T^{(0)}\ \text{at}\ t=0\,. \qquad (\alpha,\beta=1,\cdots,D) \tag{16}$$

Here t is the time, x_α is the spatial coordinate, R is the specific gas constant, and b is a given constant related to the specific-heat ratio γ by

$$\gamma=\frac{b+2}{b}. \tag{17}$$

ρ, u_α, T, p, and $\Pi_\alpha/2$ are, respectively, the density, the flow velocity in the x_α direction, the temperature, the pressure, and the energy flux in the x_α direction, of a gas.

Equations (15) indicate that ρ_r and H_α^{rc} in (8) are identified as

$$\rho_0=\rho,\ \ \rho_r=\rho u_r\ (r=1,\cdots D),\ \ \rho_{D+1}=\rho\left(bRT+u_\beta^2\right), \tag{18}$$

$$H_\alpha^{0c}=\rho u_\alpha,\ \ H_\alpha^{rc}=\rho u_r u_\alpha+p\delta_{r\alpha},\ \ H_\alpha^{D+1\,c}=\Pi_\alpha. \tag{19}$$

Accordingly, in view of (1) and (2), we let

$$\phi_0=1,\ \ \phi_\alpha=c_\alpha,\ \ \phi_{D+1}=c_\beta^2+\eta^2, \tag{20}$$

and define the macroscopic variables by

$$\rho=\int_{-\infty}^{\infty}\cdots\int_{-\infty}^{\infty} f\,d\boldsymbol{c}d\eta\,,\quad \rho u_\alpha=\int_{-\infty}^{\infty}\cdots\int_{-\infty}^{\infty} f\,c_\alpha\,d\boldsymbol{c}d\eta\,,\quad \rho(bRT+u_\beta^2)=\int_{-\infty}^{\infty}\cdots\int_{-\infty}^{\infty} f\,(c_\beta^2+\eta^2)d\boldsymbol{c}d\eta\,. \tag{21a-c}$$

f_i^c then must satisfy, from (4),

$$\rho=\int_{-\infty}^{\infty}\cdots\int_{-\infty}^{\infty} f^c d\boldsymbol{c}d\eta\,,\quad \rho u_\alpha=\int_{-\infty}^{\infty}\cdots\int_{-\infty}^{\infty} f^c c_\alpha\,d\boldsymbol{c}d\eta\,,\quad \rho(bRT+u_\beta^2)=\int_{-\infty}^{\infty}\cdots\int_{-\infty}^{\infty} f^c(c_\beta^2+\eta^2)d\boldsymbol{c}d\eta\,, \tag{22a-c}$$

$$\rho u_\alpha u_\beta+p\delta_{\alpha\beta}=\int_{-\infty}^{\infty}\cdots\int_{-\infty}^{\infty} f^c c_\alpha c_\beta d\boldsymbol{c}d\eta\,,\quad \Pi_\alpha=\int_{-\infty}^{\infty}\cdots\int_{-\infty}^{\infty} f^c(c_\beta^2+\eta^2)c_\alpha\,d\boldsymbol{c}d\eta\,. \tag{22d,e}$$

The corresponding continuous model is the Maxwellian. However, the purpose of the present study is to devise discrete molecular-velocity model. The velocity distribution function f must be the collection of delta functions of c_α and η with their center at the discrete points. Let $c_{\alpha i}$ and η_i $(i=0,1,\cdots,3I)$ be such molecular velocities c_α and η on the discrete points, and f_i and f_i^c be the corresponding coefficients of delta functions for the velocity distribution function (i.e., $f=\sum_{i=0}^{3I} f_i\delta(c_1-c_{1i},c_2-c_{2i},\cdots,\eta-\eta_i)$) and that for the Chapman-Enskog-type

distribution function, respectively. The total number of discrete molecular velocities is $3I+1$. From (21), the macroscopic variables ρ, u_α, and T are defined as

$$\rho = \sum_{i=0}^{3I} f_i, \quad \rho u_\alpha = \sum_{i=0}^{3I} f_i c_{\alpha i}, \tag{23a,b}$$

$$\rho(bRT + u_\alpha^2) = \sum_{i=0}^{3I} f_i\left(c_{\alpha i}^2 + \eta_i^2\right), \tag{23c}$$

and from (22), f_i^c should satisfy

$$\rho = \sum_{i=0}^{3I} f_i^c, \quad \rho u_\alpha = \sum_{i=0}^{3I} f_i^c c_{\alpha i}, \tag{24a,b}$$

$$\rho(bRT + u_\alpha^2) = \sum_{i=0}^{3I} f_i^c\left(c_{\alpha i}^2 + \eta_i^2\right), \tag{24c}$$

$$\rho u_\alpha u_\beta + p\delta_{\alpha\beta} = \sum_{i=0}^{3I} f_i^c c_{\alpha i} c_{\beta i}, \tag{24d}$$

$$\Pi_\alpha = \sum_{i=0}^{3I} f_i^c\left(c_{\beta i}^2 + \eta_i^2\right) c_{\alpha i}, \tag{24e}$$

where the integrals with respect to c_α and η are reduced to the summation over the discrete points because f_i and f_i^c are the collection of delta functions of c_α and η. The specific model of discrete-type f_i^c satisfying (24), which is the main achievement of this study, is given as follows:

$$f_i^c(\rho, u_\alpha, T) = \begin{cases} (b-D)p/\eta_0^2 & \text{for } i = 0, \\ W_1 F_i & \text{for } i = 1, \cdots, I, \\ W_2 F_i & \text{for } i = I+1, \cdots, 2I, \\ W_3 F_i & \text{for } i = 2I+1, \cdots, 3I, \end{cases} \tag{25a}$$

where $W_1 = \frac{v_2^2+v_3^2}{v_1^2(v_1^2-v_2^2)(v_3^2-v_1^2)}$, $W_2 = \frac{v_3^2+v_1^2}{v_2^2(v_2^2-v_3^2)(v_1^2-v_2^2)}$, $W_3 = \frac{v_1^2+v_2^2}{v_3^2(v_3^2-v_1^2)(v_2^2-v_3^2)}$, and

$$F_i = \frac{1}{D+1}\left\{\Pi_\alpha c_{\alpha i} + \left[\frac{D+2}{2}\rho u_\alpha u_\beta + \left(p - \frac{\rho u_\gamma^2}{2}\right)\delta_{\alpha\beta}\right] c_{\alpha i} c_{\beta i} + \rho u_\alpha c_{\alpha i} c_{\beta i}^2 + \frac{1}{D}\left(\rho - \frac{(b-D)p}{\eta_0^2}\right) c_{\alpha i}^2 c_{\beta i}^2\right\}. \tag{25b}$$

The discrete molecular velocities c_α and η are

$$(c_{\alpha i}, \eta_i) = \begin{cases} (0, \eta_0) & \text{for } i = 0, \\ (v_1 q_{\alpha i}, 0) & \text{for } i = 1, \cdots, I, \\ (v_2 q_{\alpha i}, 0) & \text{for } i = I+1, \cdots, 2I, \\ (v_3 q_{\alpha i}, 0) & \text{for } i = 2I+1, \cdots, 3I, \end{cases} \tag{26a}$$

where v_1, v_2, v_3 and η_0 are given positive constants which are chosen according to our convenience, and $q_{\alpha i}$ $(i = 1, \cdots, I)$ is the unit vector defined by (see Figure 1)

$$q_{\alpha i}=\begin{cases} cos\pi i\ (D=1;I=2), \\ \left(cos\dfrac{\pi i}{3},sin\dfrac{\pi i}{3}\right)\ (D=2;I=6), \\ cyc:\dfrac{1}{5^{1/4}}\left(0,\pm\sqrt{\phi},\pm\dfrac{1}{\sqrt{\phi}}\right)\ (D=3;I=12), \end{cases} \tag{26b}$$

with $\phi=\left(1+\sqrt{5}\right)/2$ and cyc representing cyclic permutation. To summarize, the process of solution for our new LB model is arranged as follows:

1. Compute $f_i^c\left(\rho^{(0)},u_\alpha^{(0)},T^{(0)}\right)$ by (25), where $\rho^{(0)}$, $u_\alpha^{(0)}$, and $T^{(0)}$ are the initial values of ρ, u_α, and T.
2. Solve the discrete-type collisionless kinetic equation for f_i $(i=0,1,\cdots,3I)$

$$\frac{\partial f_i}{\partial t}+c_{\alpha i}\frac{\partial f_i}{\partial x_\alpha}=0, \tag{27}$$

in a continuous sequence of time intervals $(0,\Delta t]$, $(\Delta t,2\Delta t]$,$\cdots$ under the following initial condition for each interval $(m\Delta t,(m+1)\Delta t]$:

$$f_i=f_i^c\left(\rho^{(m)},u_\alpha^{(m)},T^{(m)}\right). \tag{28}$$

3. If there is a boundary, the procedure on the boundary is the same as above (1 and 2) except that the impermeable condition for $u_\alpha^{(m)}$ should be imposed in (28) by $u_\alpha^{(m)}\to u_\alpha^{(m)}-\left(u_\beta^{(m)}n_\beta\right)n_\alpha$ (n_α: unit vector normal to the boundary). Note that the downwind scheme is used for the computation of (27) for $c_{\alpha i}n_\alpha>0$. We encountered no instability by this.

Then the macroscopic variables ρ, u_α, and T obtained from the solution f_i of (27) and (28) satisfy the set of compressible Euler equations, or (15) and (16) within the error of $O(\Delta t)$ which can be made sufficiently small irrespective of flow parameters. The proposed LB model (27)-(28) overcomes the issues (i) and (ii) of the current LBM, since there is no relaxation time and there is no need to store the velocity distribution function when one wants to compute a subsequent time development.

4. ERROR ESTIMATES

We here estimate the error term of the above collisionless kinetic system in terms of macroscopic variables. To this end, we utilize (14) to find that the error term of the collisionless system is

$$E_r=\frac{\Delta t^2}{2}\frac{\partial}{\partial x_\alpha}\int_{-\infty}^{\infty}\cdots\int_{-\infty}^{\infty}Q\phi_r c_\alpha d\boldsymbol{c}d\eta\quad(r=0,\cdots D+1), \tag{29}$$

where Q is the collision term defined by (5b). Q is rewritten, after substitution of (18) and (19), as

$$\begin{aligned} Q&=\frac{\partial f^c}{\partial\rho_0}\frac{\partial\rho_0(c_\beta-u_\beta)}{\partial x_\beta}+\frac{\partial f^c}{\partial\rho_\alpha}\frac{\partial\rho_\alpha(c_\beta-u_\beta)}{\partial x_\beta}+\frac{\partial f^c}{\partial\rho_{D+1}}\frac{\partial\rho_{D+1}(c_\beta-u_\beta)}{\partial x_\beta}-\left[\frac{\partial f^c}{\partial\rho_r}\frac{\partial p}{\partial x_r}+2\frac{\partial f^c}{\partial\rho_{D+1}}\frac{\partial pu_\beta}{\partial x_\beta}\right] \\ &\approx\frac{\partial f^c(c_\beta-u_\beta)}{\partial x_\beta}, \end{aligned} \tag{30}$$

where the terms in square brackets including $\partial p/\partial x_r$ and $\partial u_\alpha/\partial x_\alpha$ are ignored to derive the last equality for simplicity. Substituting (30) into (29), we find that

$$E_r \approx \frac{\Delta t^2}{2}\frac{\partial^2}{\partial x_\alpha \partial x_\beta}\int_{-\infty}^{\infty}\cdots\int_{-\infty}^{\infty} f^c \phi_r (c_\alpha - u_\alpha)(c_\beta - u_\beta) d\boldsymbol{c} d\eta$$
$$\propto \begin{cases} 0 & (r=0) \\ \Delta t^2 \dfrac{\partial^2 \rho u_r}{\partial x_\alpha^2} & (r=1,\cdots,D) \\ \Delta t^2 \dfrac{\partial^2 \rho (bRT + u_\beta^2)}{\partial x_\alpha^2} & (r=D+1) \end{cases} \tag{31}$$

where the terms including $\partial p/\partial x_r$ and $\partial u_\alpha/\partial x_\alpha$ are omitted again and $\int_{-\infty}^{\infty}\cdots\int_{-\infty}^{\infty} f^c \phi_r (c_\alpha - u_\alpha)(c_\beta - u_\beta) d\boldsymbol{c} d\eta$ ($\alpha \neq \beta$) is assumed to be small. Thus, the error term of the collisionless system is proportional to the second spatial derivatives of the macroscopic variables ρ_r multiplied by Δt^2. In the compressible Euler equations (15), these error terms correspond to 0, $\Delta t^2 \partial^2 \rho u_\alpha / \partial x_\beta^2$, and $\Delta t^2 \partial^2 \rho (bRT + u_\beta^2)/\partial x_\alpha^2$ for (15a), (15b), and (15c), respectively. These error terms work as numerical dissipation and enable us to compute supersonic flows with shock waves stably. Examples of numerical results together with discussion on the role of these error terms are given in Section 5.

5. NUMERICAL EXAMPLES

In this section, we will give several numerical examples of the LB model (27)-(28) presented in Section 3. The finite-difference scheme with the usual first-order forward in time and the third-order upwind in space (so called UTOPIA) is used for numerical computation of (27). Regarding the spatial grid generation, we solved the Poisson equation to construct the boundary-fitted curvilinear coordinate grid[37] for all computation of the two and three-dimensional flows. Calculation examples presented in this section are: (I) the one-dimensional shock-tube problem $(D = 1)$, (II) the two-dimensional supersonic flows over a wedge or a blunt body $(D = 2)$, (III) the three-dimensional supersonic flows over a cone or a sphere $(D = 3)$. We also make a comparison of our numerical results with the corresponding theoretical or other numerical solution.

5.1. Shock-tube problem

In this section, we consider the one-dimensional shock-tube problem. The initial macroscopic variables at $t = 0$ are given by

$$\rho^{(0)} = \begin{cases} \rho_1 \text{ for } x_1 < 750 \\ \rho_0 \text{ for } x_1 > 750 \end{cases}, \quad u_1^{(0)} = 0, \quad T^{(0)} = T_0, \tag{32}$$

where ρ_0, ρ_1, L, and T_0 are given positive constants. This problem is characterized by the initial density ratio ρ_1/ρ_0 and the specific heat ratio γ. We solve two schemes: (I) Our proposed new LB model (27)-(28) with $D = 1$,

(II) Roe's FDS[38] with the third-order MUSCL TVD scheme (we used the classical Roe's scheme although a new improved scheme has been developed recently by Xie et al.[39]). The number of lattice points is 1,500 and the lattice interval Δx is unity. The time interval Δt is 2.0×10^{-2}, the CFL number ($\equiv c\,\Delta t/\Delta x_{min}$: c is the sound speed) is 2.37×10^{-3}. We set the specific heat ratio $\gamma = 1.4$ (diatomic molecules) and density ratio ρ_1/ρ_0 =10. Figure 2 shows a comparison between the result ρ/ρ_1 of our proposed new LB model and Roe's FDS[38]. New LB model can capture sharply the shock and contact discontinuity in approximately 2 or 3 grids as in the Roe's FDS[38]. Although the numerical results of new LB model have small overshoot near the discontinuities, we find a good agreement between two numerical results.

Regarding a comparison with the current LB model, we did a comparison against the results by Li et al.[9]. They devised the so called coupled double-distribution function LB method and computed the shock-tube problem for a little different initial conditions from above: ρ_1/ρ_0 =8 and p_1/p_0 (pressure ratio) =10. Their density result is shown in figure 2(a) of their paper (Ref.9), which indicates that the shock wave and contact discontinuity are a little smoothed out and spanned over 4 to 6 grids. This dissipation occurs for any current LB models because there is no BGK-type model that can compute an inviscid flow as mentioned in Section 1 (defect (i) of current LB models). A small finite viscosity must be always added to compute any inviscid flows by the current LB models, while our new model can reduce the numerical dissipation as small as possible by choosing small Δt.

5.2. Two-dimensional supersonic flows over a wedge or brunt body

In this section, we calculate the two-dimensional supersonic flow over a wedge or brunt body (circular cylinder) using our proposed new LB model with $D = 2$.

First, we consider supersonic flow over a wedge. This problem is characterized by the specific heat ratio γ, upstream Mach number $M_0\left(= u_0/\sqrt{\gamma RT_0}\right)$ and the wedge angle θ_w. The specific heat ratio γ is fixed at 1.4 (diatomic molecules). We computed the cases of $M_0 = 2.5,\ 3.4,\ 4.2,$ and 5.1 with $\theta_w = 10°,\ 20°,$ and $30°$ until numerical results reach a steady state. Figure 3 shows non-dimensional pressure distribution p/p_0 for (a) $M_0 = 4.2, \theta_w = 10°$ and (b) $M_0 = 5.1, \theta_w = 30°$. New LB model with $D = 2$ can simulate stably supersonic flows over a wedge for $M_0 \leq 5.1$ when wedge angle is $\theta_w = 30°$, and it captures the shock in approximately 4-8 grids. Figure 4 shows a comparison between numerical results and the oblique shock theory in terms of shock angle β_w versus wedge angle θ_{w}. We find a good agreement between numerical results and theoretical values.

Next, let us consider supersonic flows over a brunt body (circular cylinder). This problem is characterized by the specific heat ratio γ and upstream Mach number $M_0\left(= u_0/\sqrt{\gamma RT_0}\right)$. It is well known that detached shock occurs in supersonic flow over brunt body. The standoff distance of circular cylinder δ_{c} is predicted experimentally by Billig[40]. We computed for $M_0 = 1.7, 2.0, 2.5, 3.0, 3.4, 4.2$ at fixed $\gamma = 1.4$. Figure 5 shows non-dimensional pressure distribution p/p_0 for (a) $M_0 = 1.7$ and (b) $M_0 = 4.2$. New LB model can simulate stably supersonic flows over a circular cylinder for $M_0 \leq 4.2$. New LB model capture the shock in approximately 3-4 grids. Figure 6

shows a comparison between numerical results and experiments by Billig[40] in terms of non-dimensional standoff distance δ_c/L_c (L_c: diameter of cylinder) versus upstream Mach number M_0. We find a good agreement between numerical results and experiments by Billig.

5.3. Three-dimensional supersonic flows over a cone or sphere

In this section, we calculate the three-dimensional supersonic flow over a cone or sphere using our proposed new LB model with $D = 3$.

First, we consider supersonic flows over a cone. This problem is characterized by the upstream Mach number $M_0\left(= u_0/\sqrt{\gamma RT_0}\right)$, half the apex angle of cone θ_c, and the specific heat ratio γ. We set $M_0 = 2.0, 2.5, 3.0, 3.5, 4.0, 4.5$, and $\theta_c = 10°, 20°$ and $30°$ for fixed $\gamma = 1.4$. Figure 7 shows non-dimensional pressure distribution p/p_0 for (a) $M_0 = 4.0, \theta_c = 10°$ and (b) $M_0 = 4.0, \theta_c = 30°$. New LB model can simulate stably supersonic flows over a cone for $M_0 \leq 4.0$ when $\theta_c = 30°$, and captures the shock in approximately 4-9 grids. Figure 8 shows a comparison between numerical results and the Taylor-Maccoll theory[42,43] in shock angle β_c versus upwind Mach number M_0. Although for $\theta_c = 30°$ numerical results underrun theoretical values, which is caused by weak damping due to numerical viscosity of new LB model with $D = 3$ under rough spatial mesh distribution, for $\theta_c = 10°$ and $20°$ we see a good agreement between numerical results and theoretical values.

Finally, we treat supersonic flows over a sphere. This problem is characterized by the specific heat ratio γ and upstream Mach number $M_0\left(= u_0/\sqrt{\gamma RT_0}\right)$. It is well known that the detached shock occurs in supersonic flows over a sphere. The standoff distance δ_s of a sphere is predicted experimentally by Billig[40] as in the case of the circular cylinder. Figure 9 shows the non-dimensional pressure distribution p/p_0 for $\gamma = 1.4$ when (a) $M_0 = 1.8$ and (b) $M_0 = 2.5$. New LB model capture the shock in approximately 4 or 5 grids. Figure 10 shows a comparison between numerical results and experimental values by Billig in terms of the non-dimensional standoff distance δ_s/L_s (L_s: diameter of sphere) versus the upstream Mach number M_0. The shock around sphere is thicker than that around a circular cylinder due to the lattice viscosity of rough spatial mesh distributions. However, we find a good agreement between numerical results and experiments by Billig.

6. CONCLUSION

We have developed a new type of LB model that gives solution of the compressible Euler equations on the basis of the collisionless kinetic-equation approach proposed by Sone. This LB model overcomes all the defects (i) and (ii) of current LBM mentioned in Section 1. Compared with another line of studies called the gas-kinetic schemes, our model has the merit of 'simpleness' because we only have to solve the simple kinetic equation and there is no need for reconstruction process. These metis of our scheme are summarized in (I)-(III) of Section 1. We calculated various inviscid supersonic flows associated with shock waves by our new model and find a good agreement with some established theory and numerical solution. Thus, our new model can be a new fundamental LB model which replaces the current LB models.

ACKNOWLEDGEMENTS

This work was partially supported by JSPS KAKENHI Grant No. 18K03930.

DATA AVAILABILITY STATEMENT

The data that support the findings of this study are available from the corresponding author upon reasonable request.

REFERENCE

1. Sone, Y. *Kinetic Theory and Fluid Dynamics*. Birkhäuser: Boston, 2002.
2. Alexander, F. J., Chen, S., Sterling, J. D. Lattice Boltzmann thermohydrodynamics. *Physical Review E* 1993; **47**: R2249-2252.
3. Chen, Y., Ohashi, H., Akiyama, H. Thermal lattice Bhatnagar-Gross-Krook model without nonlinear deviations in macrodynamic equations. *Physical Review E* 1994; **50**: 2776-2783.
4. McNamara, G. R., Garcia, A. L., Alder, B. J. Stabilization of thermal lattice Boltzmann models. *Journal of Statistical Physics* 1997; **87**: 395-408.
5. Chen, S., Doolen, G. D. Lattice Boltzmann method for fluid flows. *Annual Review of Fluid Mechanics* 1998; **30**: 329-364.
6. Kataoka, T., Tsutahara, M. Lattice Boltzmann model for the compressible Navier-Stokes equations with flexible specific-heat ratio. *Physical Review E* 2004; **69**: 035701(R).
7. Kataoka, T., Tsutahara, M. Lattice Boltzmann method for the compressible Euler equations. *Physical Review E* 2004; **69**: 056702.
8. Qu, K., Shu, C., Chew, Y. T. Alternative method to construct equilibrium distribution functions in lattice-Boltzmann method simulation of inviscid compressible flows at high Mach number. *Physical Review E* 2007; **75**: 036706.
9. Li, Q., He, Y. L., Wang, Y., Tao, W. Q. Coupled double-distribution-function lattice Boltzmann method for the compressible Navier-Stokes equations. *Physical Review E* 2007; **76**: 056705.
10. Prasianakis, N. I., Karlin, I. V. Lattice Boltzmann method for simulation of compressible flows on standard lattices. *Physical Review E* 2007; **78**: 016704.
11. Gan, Y., Xu, A., Zhang, G., Yu, X., Li, Y. Two-dimensional lattice Boltzmann model for compressible flows with high Mach number. *Physica A: Statistical Mechanics and its Applications* 2008; **387**: 1721-1732.
12. Li, Q., He, Y., Wang, Y., Tang, G. Three-dimensional non-free-parameter lattice-Boltzmann model and its application to inviscid compressible flows. *Physics Letters A* 2009; **373**: 2101-2108.
13. Chen, F., Xu, A. G., Zhang, G. C., Li, Y. J. Three-dimensional lattice Boltzmann model for high-speed

compressible flows. *Communications in Theoretical Physics* 2010; **54**: 1121-1128.

14. Yang, L. M., Shu, C., Wu, J. Development and comparative studies of three non-free parameter lattice Boltzmann models for simulation of compressible flows. *Advances in Applied Mathematics and Mechanics* 2012; **4**: 454–472.
15. Li, K., Zhong, C. A lattice Boltzmann model for simulation of compressible flows. *International Journal for Numerical Methods in Fluids* 2015; **77**: 334–357.
16. Qiu, R. F., You, Y. C., Zhu, C. X., Chen, R. Q. Lattice Boltzmann simulation for high-speed compressible viscous flows with a boundary layer. *Applied Mathematical Modelling* 2017; **48**: 567–583.
17. Dellar, P. J. Two routes from the Boltzmann equation to compressible flow of polyatomic gases. *Progress in Computational Fluid Dynamics, an International Journal* 2008; **8**: 84–96.
18. Tsutahara, M., Kurita, M. Kataoka, T. Direct simulation of acoustic waves by the finite difference lattice Boltzmann method. *Transactions of the Japan Society of Mechanical Engineers Series B* 2003; **69**: 841-847 (in Japanese).
19. Tsutahara, M., Kataoka, T., Shikata, K., Takada, N. New model and scheme for compressible fluids of the finite difference lattice Boltzmann method and direct simulations of aerodynamic sound. *Computers and Fluids* 2008; **37**: 79-89.
20. Tamura, A., Tsutahara, M., Kataoka, T., Aoyama, T., Yang, C. Numerical simulation of two-dimensional blade-vortex interactions using finite difference lattice Boltzmann method. *AIAA Journal* 2008; **46**: 2235-2247.
21. Kataoka, T., Hanada, T. New lattice Boltzmann model for the compressible Navier-Stokes equations. *International Journal for Numerical Methods in Fluids* 2019; **91**: 183-197.
22. Chen, F., Xu, A. G., Zhang, G. C., Li, Y. J., Succi, S. Multiple-relaxation-time lattice Boltzmann approach to compressible flows with flexible specific-heat ratio and Prandtl number. *Europhysics Letters.* 2010; **90**(5): 54003.
23. Chen, F., Xu, A., Zhang, G. C., Li, Y. J. Multiple-relaxation-time lattice Boltzmann model for compressible fluids. *Physics Letters. A* 2011; **375**(21): 2129–2139.
24. Inamuro, T. A lattice kinetic scheme for incompressible viscous flows with heat transfer. *Philosophical Transactions of the Royal Society of London A* 2002; **360**: 477-484.
25. Pullin, D. I. Direct simulation methods for compressible inviscid ideal-gas flow. *Journal of Computational Physics* 1980; **34**: 231-244.
26. Mandal, J. C., Deshpande, S. M. Kinetic flux vector splitting for Euler equations, *Computers and Fluids* 1994; **23**: 447-478.
27. Chou, S. Y., Baganoff, D. Kinetic Flux–Vector Splitting for the Navier–Stokes Equations. *Journal of Computational Physics* 1997; **130**: 217-230.
28. Chae, D., Kim, C., Rho, O. H. Development of an improved gas-kinetic BGK scheme for inviscid and viscous flows, *Journal of Computational Physics* 2000; **158**: 1-27.
29. Xu, K. A gas-kinetic BGK scheme for the Navier-Stokes equations and its connection with artificial dissipation

and Godunov method, *Journal of Computational Physics* 2001; **171**, 289-335.

30. Jiang, J., Qian, Y. Implicit gas-kinetic BGK scheme with multigrid for 3D stationary transonic high-Reynolds number flows, *Computers and Fluids* 2012; **66**: 21-28.
31. Ohwada, T. On the construction of kinetic schemes, *Journal of Computational Physics* 2002; **177**, 156-175.
32. Li, Q., Xu, K., Fu, S. A high-order gas-kinetic Navier–Stokes flow solver, *Journal of Computational Physics* 2010; **229**, 6715-6731.
33. Zhou, G., Xu, K., Liu, F. Simplification of the flux function for a high-order gas-kinetic evolution model, *Journal of Computational Physics* 2017; **339**, 146-162.
34. Ji, X., Pan, L., Shyy, W., Xu, K. A compact fourth-order gas-kinetic scheme for the Euler and Navier–Stokes equations, *Journal of Computational Physics* 2018; **372**, 446-472.
35. Yang, L. M., Shu, C., Wu, J., Zhao, N., Lu, Z. L. Circular function-based gas-kinetic scheme for simulation of inviscid compressible flows, *Journal of Computational Physics* 2013; **255**, 540-557.
36. Yang, L. M., Shu, C., Yang, W. M., Wang, Y., Wu, J. An immersed boundary-simplified sphere function-based gas kinetic scheme for simulation of 3D incompressible flows, *Physics of Fluids* 2017; **29**, 083605.
37. Fletcher, C. A. J. *Computational Techniques for Fluid Dynamics Vol.II*. Springer, 1991.
38. Roe, P. L., Approximate Riemann solvers, parameter vectors, and difference schemes, *Journal of Computational. Physics.* 1981; **43:** 357-372.
39. Xie, W., Zhang, Y., Chang, Q., Li, H. Towards an accurate and robust Roe-type scheme for all Mach number flows, *Advances in Applied Mathematics and Mechanics* 2019; **11**, 132-167.
40. Billig, F. S. Shock-wave shapes around spherical-and cylindrical-nosed bodies. *Journal of Spacecraft and Rockets*.1967; **4**: 822-823.
41. Yang, L. M., Shu, C., Wu, J. A hybrid lattice Boltzmann flux solver for simulation of viscous compressible flows. *Advances in Applied Mathematics and Mechanics* 2016; **8**, 887-910.
42. Taylor, G. I., Maccoll, J. W. The Air Pressure on a cone Moving at High Speeds, *Proc. Roy. Soc.* A 1933, **139**: 278-311.
43. Maccoll, J. W. The Conical Shock Wave Formed by a Cone Moving at High Speed, *Proc. Roy. Soc.* A 1937; **159**: 459.

FIGURE CAPTIONS

Fig.1. Distribution of the unit vector $q_{\alpha i}$ $(\alpha = 1, \cdots, D;\ i = 1, \cdots, I)$ for the discrete molecular velocities $c_{\alpha i}$ of D dimensional model: (a) one-dimensional model $(D = 1, I = 2)$, (b) two-dimensional model $(D = 2, I = 6)$; (c) three-dimensional model $(D = 3, I = 12)$.

Fig.2. Numerical results ρ/ρ_1 for the shock-tube problem whose initial condition is (32), when $\rho_1/\rho_0 = 10$ and $\gamma = 1.4$. The triangles and squares represent numerical results of the new LB model and Roe's FDS[38], respectively.

Fig.3. Non-dimensional pressure distribution p/p_0 of supersonic flows over a wedge calculated by new LB model (27)-(28) with $D = 2$ for $\gamma = 1.4$: (a) $M_0 = 4.2$ and $\theta_w = 10°$, (b) $M_0 = 5.1$ and $\theta_w = 30°$.

Fig.4. Comparison of numerical results with theoretical values on angle β_w of shock waves versus wedge angles θ_w for various upwind Mach numbers M_0. The solid line represents the analytical solution of the oblique shock theory. The points are results by the new LB model (□: $M_0 = 2.5$, △: 3.4, ◇: 4.2, ○: 5.1) .

Fig.5. Non-dimensional pressure distributions p/p_0 of the supersonic flows over a circular cylinder calculated by the new LB model for $\gamma = 1.4$: (a) $M_0 = 1.7$; (b) $M_0 = 4.2$.

Fig.6. Comparison of numerical results with experiments on the non-dimensional standoff distance δ_c/L_c versus the upwind Mach number M_0. The solid line represents experimental results by Billig[41] and the circles are numerical results of the new LB model.

Fig.7. Non-dimensional pressure distribution p/p_0 of the supersonic flows over a cone calculated by the new LB model (27)-(28) with $D = 3$ for $M_0 = 4.0$ and $\gamma = 1.4$: (a) $\theta_c = 10°$, (b) $\theta_c = 30°$.

Fig.8. Comparison of numerical results with theoretical values on angle β_c of shock waves versus cone angles θ_c for various upwind Mach numbers M_0. The solid line represents the analytical solution of the Taylor-Maccoll theory[42,43]. The points are results of the new LB model for $\theta_c = 10°, 20°$ and $30°$.

Fig.9. Non-dimensional pressure distributions p/p_0 of the supersonic flows over a sphere calculated by the new LB model for $\gamma = 1.4$: (a) $M_0 = 1.8$; (b) $M_0 = 2.5$.

Fig.10. Comparison of numerical results with experiments on the non-dimensional standoff distance δ_s/L_s versus the upwind Mach number M_0. The solid line represents Billig[41]. The squares are results of the new LB model for

M_0 =1.5, 1.8, 2.0, 2.3 and 2.5, respectively. The two squares connected by a vertical line correspond to the start and end points of shock waves.

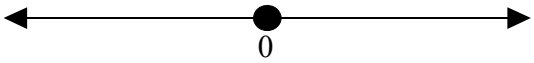

(a)

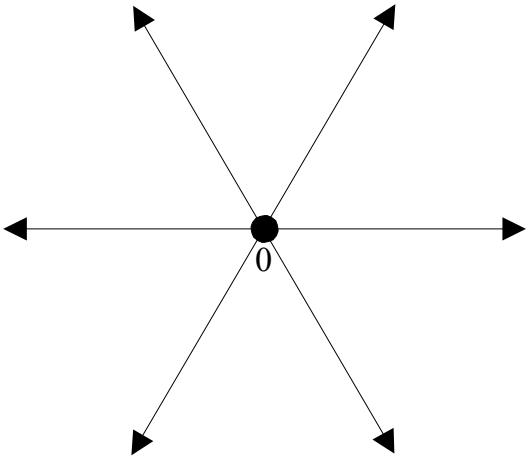

(b)

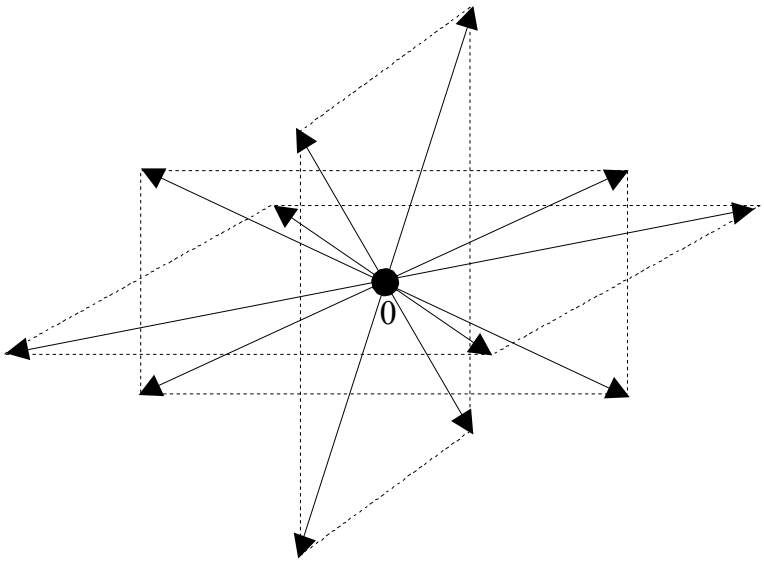

(c)

Figure.1

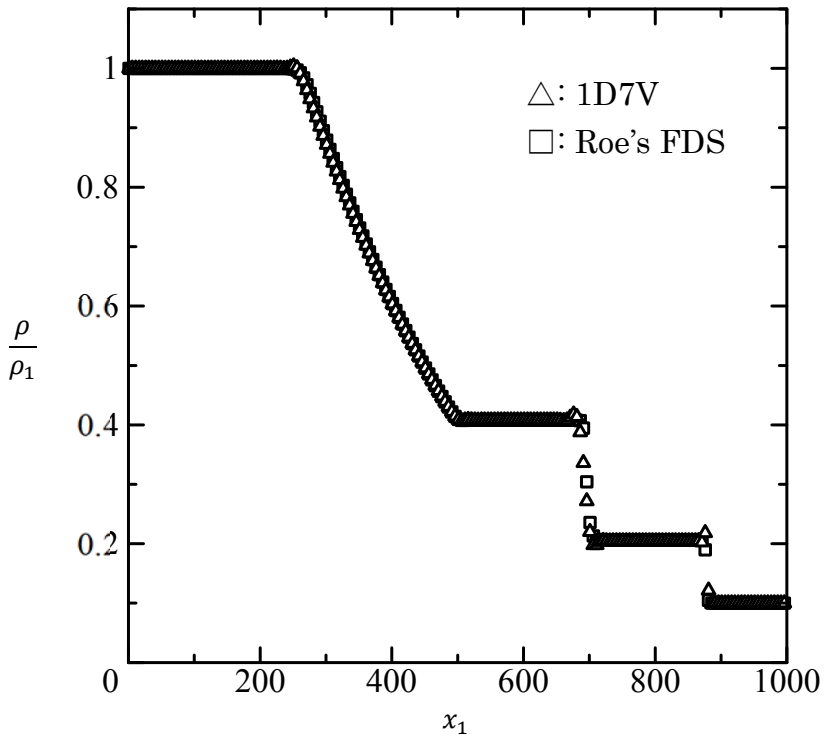
△: 1D7V
□: Roe's FDS
1
0.8
0.6
0.4
0.2
0
200
400
600
800
1000
$\frac{\rho}{\rho_1}$
x_1

Figure.2

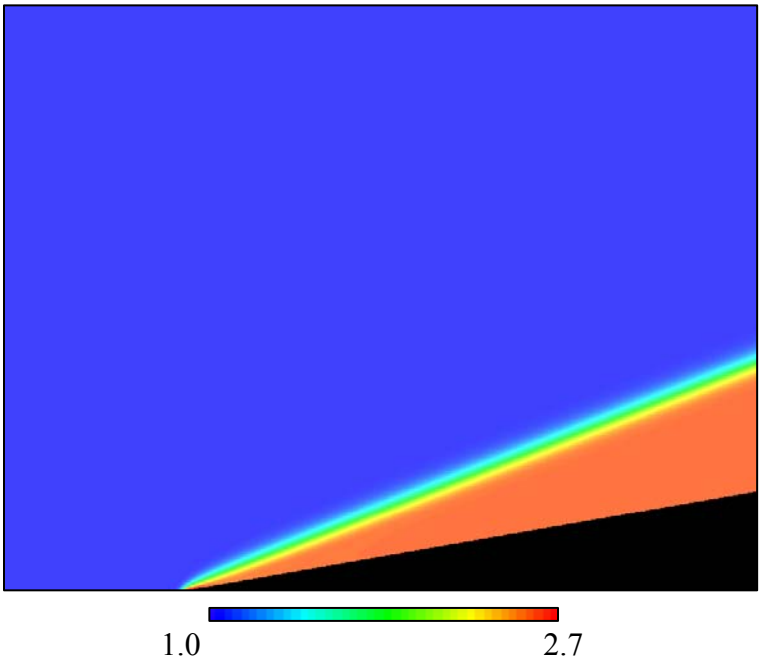

(a)

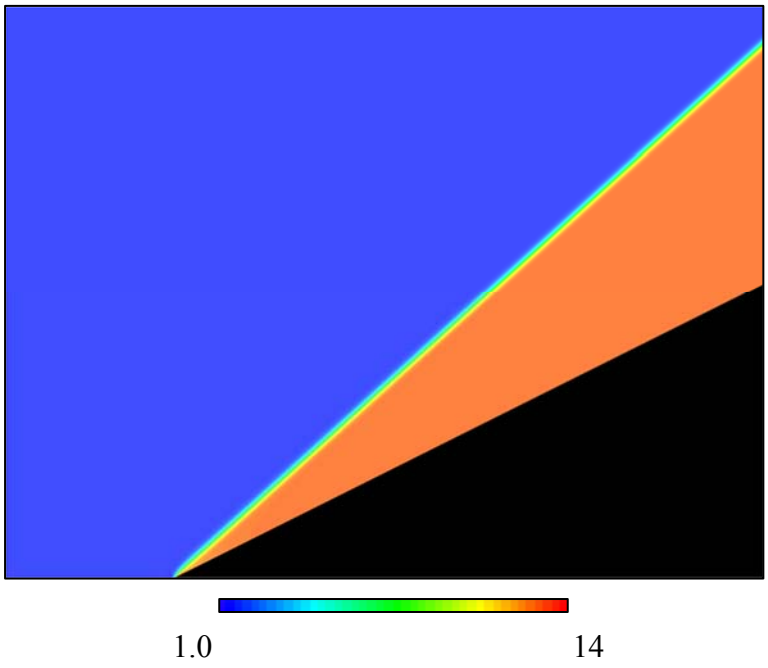

(b)

Figure.3

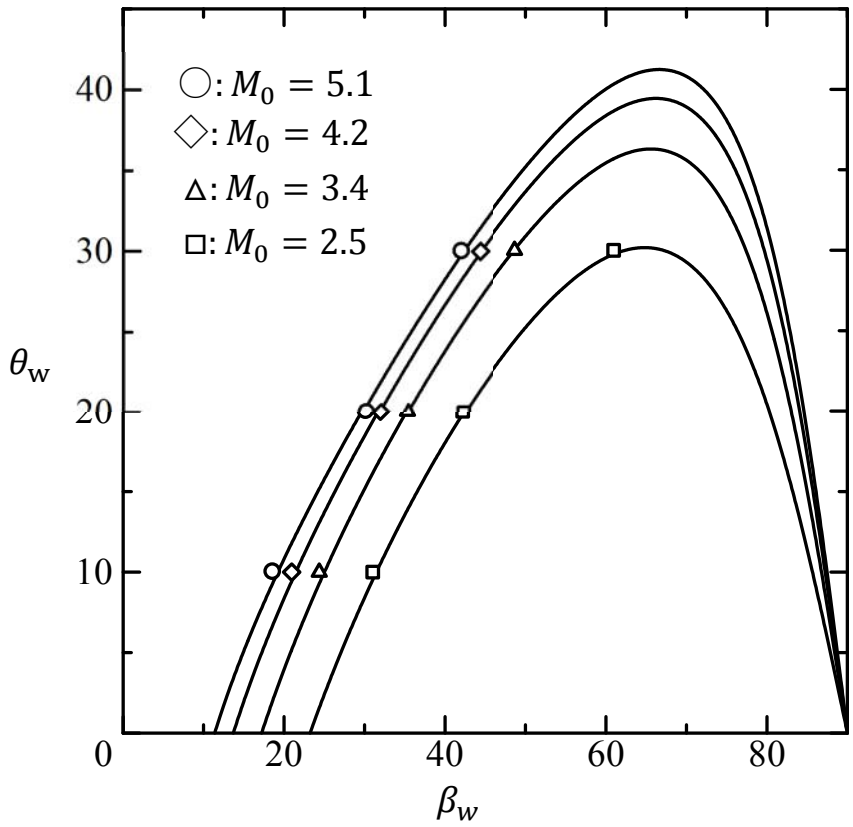

Figure.4

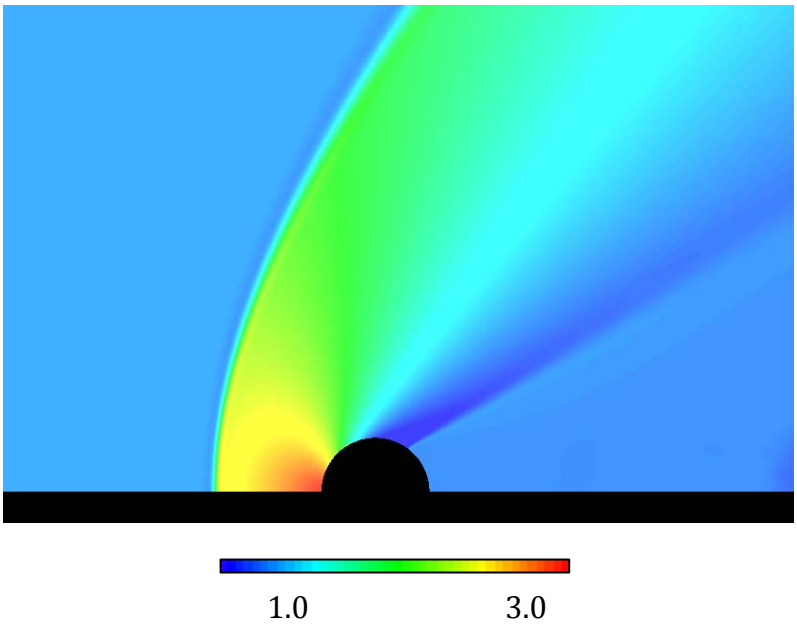

(a)

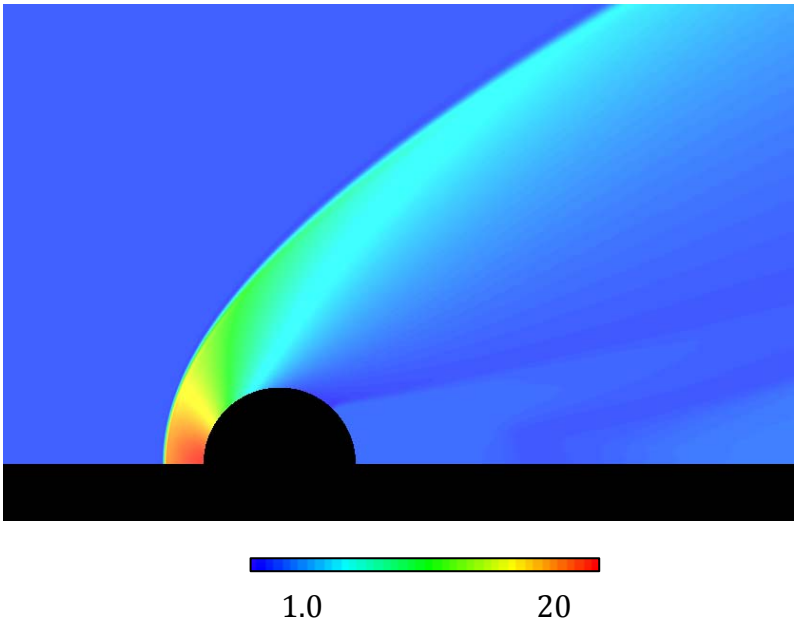

(b)

Figure.5

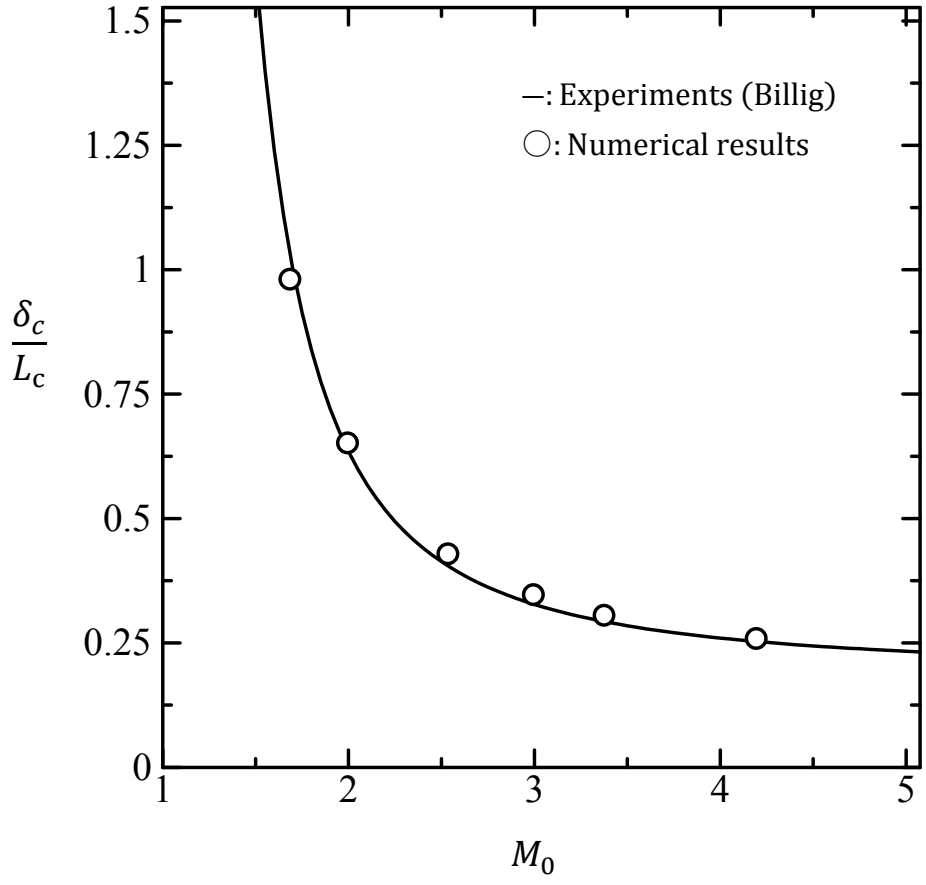
1.5
1.25
1
0.75
0.5
0.25
0
1
2
3
4
5
—: Experiments (Billig)
○: Numerical results
$\frac{\delta_c}{L_c}$
M_0

Figure.6

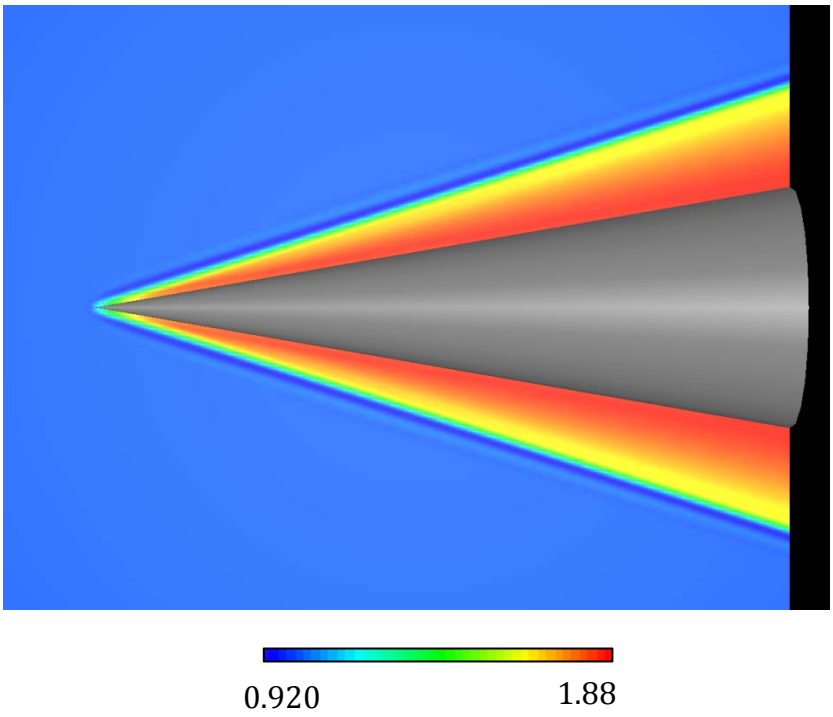

(a)

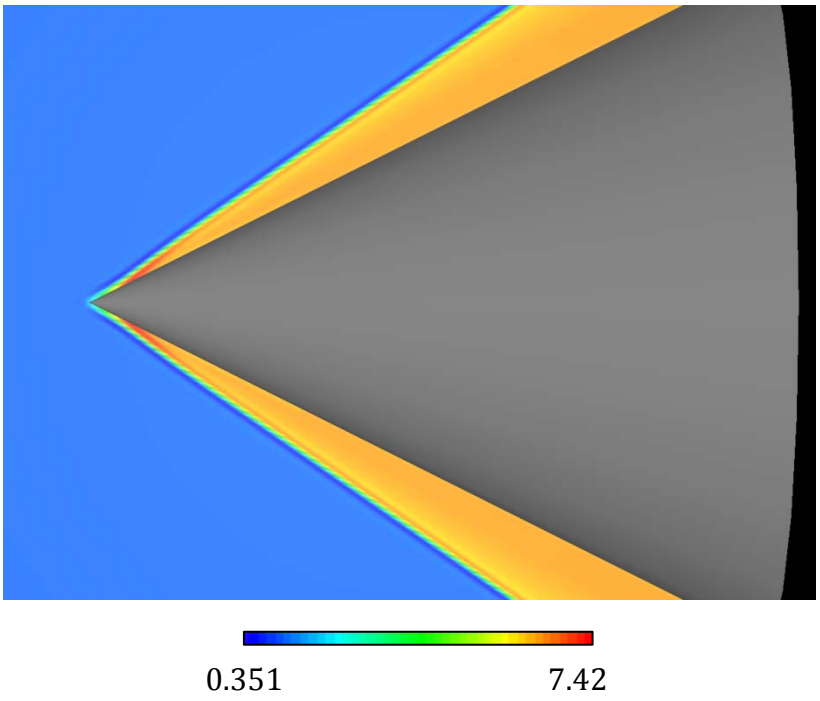

(b)

Figure.7

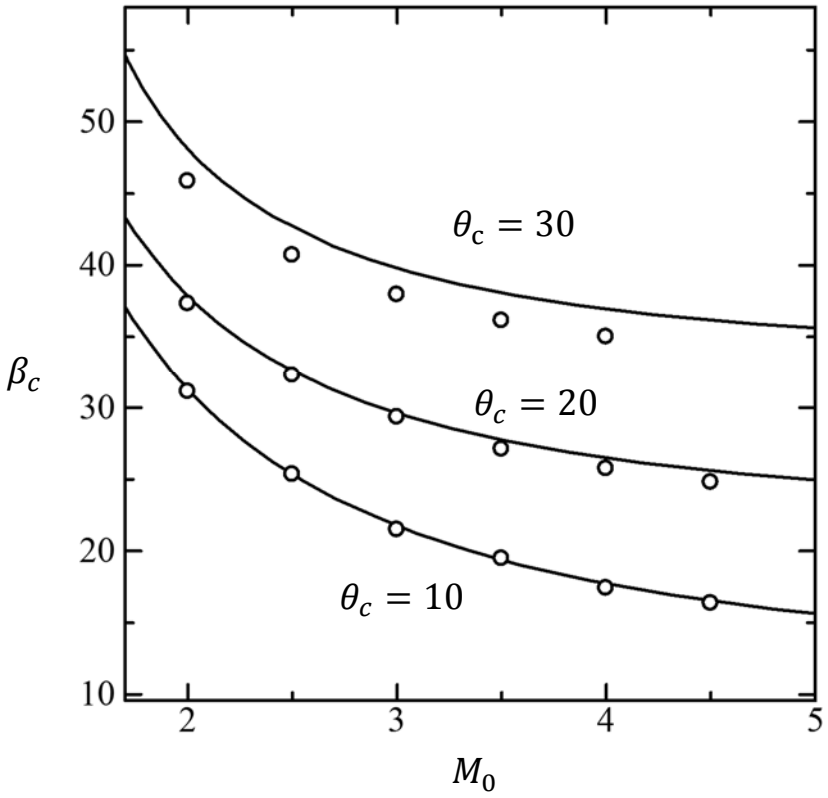

Figure.8

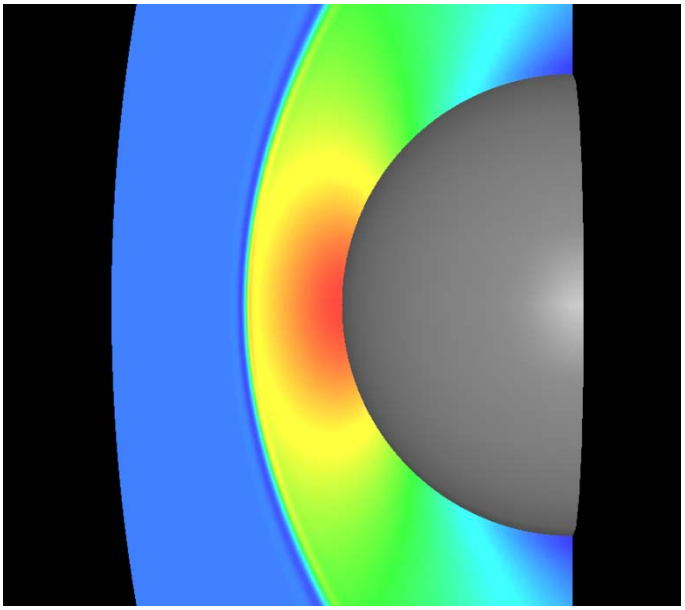

(a)

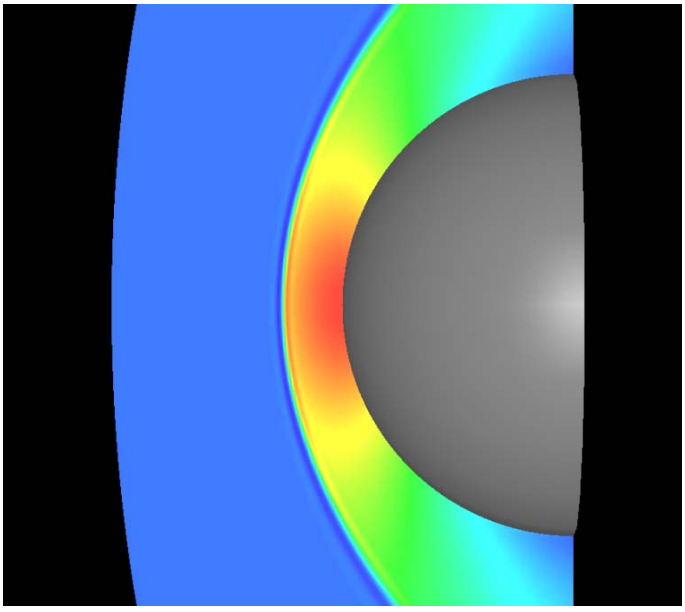

(b)

Figure 9

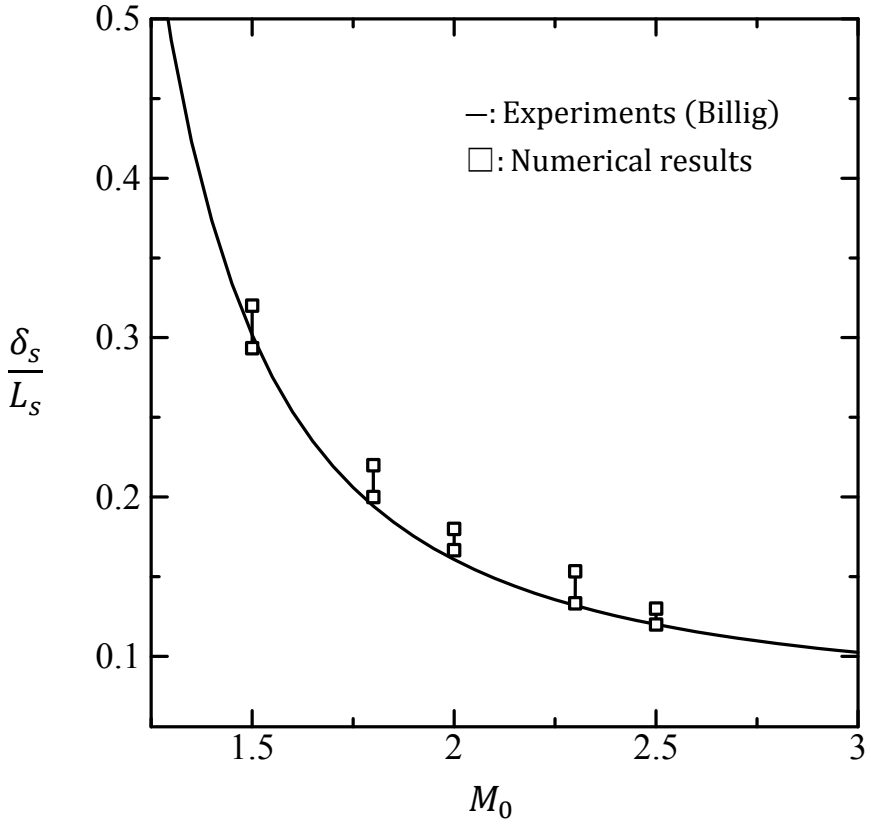
0.5
0.4
0.3
0.2
0.1
$\frac{\delta_s}{L_s}$
—: Experiments (Billig)
□: Numerical results
1.5
2
2.5
3
M_0

Figure.10